Energy-Flow Dynamics in the Molecular Channel of Propanal Photodissociation, $C_2H_5CHO \rightarrow C_2H_6 + CO$: Direct ab Initio Molecular Dynamics Study

Yuzuru Kurosaki[†]

Kansai Photon Science Institute, Japan Atomic Energy Agency, Kizu, Kyoto 619-0215, Japan

Received: June 4, 2006; In Final Form: August 8, 2006

Direct ab initio molecular dynamics calculations have been carried out for the molecular channel of the photodissociation of propanal, $C_2H_5CHO \rightarrow C_2H_6 + CO$, at the RMP2(full)/cc-pVDZ level of ab initio molecular orbital theory. The initial conditions were generated using the microcanonical sampling to put the excess energy randomly into all vibrational modes of the TS. Starting from the TS, a total of ∼700 trajectories were numerically integrated for 100 fs. The obtained final energy distributions for the C_2H_6 and CO fragments and their relative translational motion were found to be quite similar to those obtained for the acetaldehyde reaction, $CH_3CHO \rightarrow CH_4 + CO$, in our previous study (*Chem. Phys. Lett.* **2006**, *421*, 549) despite the fact that the number of degree of freedom for C_2H_6 is larger than that for CH_4. The coupling between the intrinsic reaction coordinate and one of the generalized normal modes orthogonal to it was predicted substantially strong around $s = 1.4$ amu$^{1/2}$ bohr, and it is expected that the energy flow out of C_2H_6 proceeds through this coupling. However, the obtained energy distributions strongly suggest that the coupling among the modes in C_2H_6 is quite small and the intramolecular energy redistribution does not occur efficiently in this molecule.

1. Introduction

Photochemistry of aliphatic aldehydes has been a major subject in the field of organic photochemical science for more than half a century.[1−35] These molecules are known to be present in the atmosphere;[2] they enter the environment from automobile exhaust or through photooxidation of organic compounds. There are two major photodissociation pathways in their photochemistry in the UV region:

$$RCHO \rightarrow RH + CO \quad (1)$$

$$\rightarrow R + HCO \quad (2)$$

where R is an alkyl group. Channels 1 and 2 are called molecular and radical channels, respectively.

The mechanisms of these two photodissociation channels have been fully elucidated.[1] In the UV region aldehydes are excited to the singlet state (S_1) from the ground singlet state (S_0) through an n−π* transition and the excited aldehydes in the S_1 state decay to the S_0 state with a fluorescence emission or undergo photodissociation. Photodissociation of aldehydes is indirect because the C−O bond still remains strong after the n−π* transition. Therefore, several photodissociation pathways in the S_1 state are possible including the two major channels. In the molecular channel excited aldehydes in the S_1 state transfer to the highly vibrationally excited states of S_0 through internal conversion, and they surmount a relatively high potential barrier yielding the molecular products RH and CO. In the radical channel excited aldehydes transfer to the lowest triplet state (T_1) through intersystem crossing and they surmount a relatively small potential barrier yielding the radical products R and HCO. It has been well established that the ground S_0 surface correlates to molecular products with a considerably high potential barrier and the T_1 potential surface does to radical products with a smaller potential barrier. It should be noted that the radical channel plays an important role in the photochemical smog cycles in the urban atmosphere.[3]

A lot of work has been devoted to the study of photochemistry of acetaldehyde[4−24] and propanal (or propionaldehyde, C_2H_5-CHO),[25−35] although much less studies have been done for propanal. Previously, we focused on the molecular channel for photodissociation of acetaldehyde, $CH_3CHO \rightarrow CH_4 + CO$,[18,19] and carried out direct ab initio molecular dynamics (MD) calculations at the RMP2(full)/cc-pVDZ level of theory. In the prior work[18] we calculated a total of 100 trajectories starting from the transition state (TS) and obtained the products (CH_4 + CO) energy distributions and the vibrational and rotational state distributions of the CO molecule. As a result, the CO state distributions were found to be consistent with the experiment of Gherman et al.[15] Since there was a serious problem in this study that the excess energy at the TS was added only to the reaction coordinate for all trajectories, we[19] later improved this calculation by integrating a lot more trajectories, ∼700, and by sampling the initial conditions microcanonically to randomly distribute the excess energy to all vibrational modes of the TS. It was surprising to see that the product energy and state distributions obtained in the latter were quite similar to the ones obtained in the former despite a significant difference in initial condition. We then calculated the curvature of the intrinsic reaction coordinate (IRC) and discovered that it becomes considerably large at some point on the way from the TS to the products. It was also found that this large curvature is composed of almost one coupling constant between the IRC and one of the generalized normal modes that correlates with a vibrational mode of CH_4. This result strongly suggests that there is a substantial energy flow between the mode of CH_4 and the IRC, which explains the independence of the final energy distribution on the initial condition.

In the present work we have carried out direct ab initio MD calculations for the molecular channel of propanal photodissociation, $C_2H_5CHO \rightarrow C_2H_6 + CO$, at 248 nm. One easily expects

[†] E-mail address: kurosaki.yuzuru@jaea.go.jp.

10.1021/jp063452s CCC: $33.50
Published on Web 09/07/2006

TABLE 1: Harmonic Vibrational Frequencies for the RMP2(full)/cc-pVDZ Geometries

sym		frequency/cm^{-1}					ZPE/hartree
C_2H_5CHO	C_s	146 (a″)	252 (a″)	263 (a′)	673 (a′)	679 (a″)	0.085 45
		888 (a′)	904 (a″)	1013 (a′)	1130 (a′)	1147 (a″)	
		1283 (a″)	1374 (a′)	1410 (a′)	1424 (a′)	1455 (a′)	
		1496 (a″)	1500 (a′)	1793 (a′)	2950 (a′)	3079 (a′)	
		3106 (a′)	3127 (a″)	3207 (a′)	3208 (a″)		
C_2H_6	D_{3d}	334 (a_{1u})	825 (e_u)	825 (e_u)	1044 (a_{1g})	1244 (e_g)	0.075 82
		1244 (e_g)	1400 (a_{2u})	1433 (a_{1g})	1506 (e_g)	1506 (e_g)	
		1507 (e_u)	1507 (e_u)				
CO	$C_{\infty v}$	2117 (σ)					0.004 82
TS	C_s	1756i (a′)	74 (a″)	145 (a′)	166 (a″)	296 (a′)	0.078 75
		535 (a″)	655 (a′)	856 (a″)	916 (a′)	928 (a″)	
		1060 (a′)	1116 (a′)	1228 (a″)	1398 (a′)	1443 (a′)	
		1488 (a′)	1503 (a″)	1840 (a′)	3055 (a′)	3086 (a′)	
		3134 (a′)	3148 (a″)	3323 (a′)			

TABLE 2: Total Energies for the RMP2(full)/cc-pVDZ Geometries (hartree)

	state	RMP2(full)/cc-pVDZ	RMP4(SDTQ,full)/cc-pVTZ	RQCISD(T,full)/cc-pVTZ
C_2H_5CHO	$^1A'$	−192.57842	−192.89237	−192.88903
C_2H_6	$^1A_{1g}$	−79.54289	−79.70677	−79.70743
CO	$^1\Sigma^+$	−113.04085	−113.18638	−113.18097
TS	$^1A'$	−192.43448	−192.75259	−192.74661

that its dynamics is quite similar to the one for the acetaldehyde photodissociation. Since the number of degree of freedom for C_2H_6 is twice as large as that for CH_4, however, there should be a significant difference in the energy-flow dynamics between the two reactions. It is therefore worth comparing the two reactions to help understand the molecular-channel dynamics of aldehyde photodissociation.

2. Methods of Calculation

Geometries for all stationary points in the title reaction were optimized and their harmonic vibrational frequencies were obtained by diagonalizing the analytical Hessian at the RMP2-(full)/cc-pVDZ level of theory. To confirm the reliability of this theoretical level more accurate single-point energy calculations were carried out for the optimized geometries at the RMP4-(SDTQ,full)/cc-pVTZ and RQCISD(T,full)/cc-pVTZ levels of theory and the results were compared with the RMP2(full) result. In addition, the IRC and the generalized normal modes orthogonal to it and the IRC curvature was obtained. These calculations were done using the GAUSSIAN98 program package.[36]

All trajectories were started from the TS toward the products with the excess energy of 0.04648 hartree (29.2 kcal mol^{-1}) that corresponds to the difference between the photon energy at 248 nm (115.3 kcal mol^{-1}) and the reaction barrier height of 86.1 kcal mol^{-1} calculated at the RMP2(full)/cc-pVDZ level with the zero-point-energy (ZPE) correction; i.e., not only the vibrational and reaction-coordinate energies of 29.2 kcal mol^{-1} but ZPEs of the normal modes were added to the TS's degrees of freedom in the initial conditions. With the result of the harmonic vibrational analysis for the TS, the initial conditions were generated by distributing the excess energy of 29.2 kcal mol^{-1} randomly among the vibrational and reaction-coordinate degrees of freedom using classical microcanonical sampling, where a correction for the anharmonicity of molecular Hamiltonian was considered.[37] Thus, the energy given to each degree of freedom for the TS in the initial conditions is the sum of the distributed excess energy and its intrinsic ZPE. A random phase was given to each normal mode in the initial conditions, but the zero phase was added to the normal mode corresponding to the reaction coordinate and its momentum was set toward product. The total angular momentum of the system was set to zero. Although the initial conditions were chosen with the classical method in the present study, a better sampling procedure that can more accurately represent experiment would be to use the quasiclassical method such as the one described by Sun and Hase,[38] which includes ZPE and gives equal probabilities of being populated to each of the TS's vibrational and rotational levels. Trajectories were numerically integrated under the condition that the total energy is kept constant. Numerical integration for Hamilton equation of motion was carried out using the fourth-order Runge−Kutta and sixth-order Adams−Bashforth−Moulton predictor−corrector methods. Analytical energy gradients[39,40] were directly obtained at every step from the ab initio molecular orbital (MO) computation at the RMP2(full)/cc-pVDZ level[41] using the MOLPRO program package.[42] Trajectories were integrated for 100 fs when the distance between the centers of mass of the products reaches ∼10 bohr. The time step of integration was 0.1 fs and ∼700 trajectories were calculated. Using a parallel computer system, each trajectory was assigned to each CPU, and many trajectories were computed at the same time.

3. Results and Discussion

A. Geometry and Energetics. Tables 1 and 2 list the harmonic vibrational frequencies at the RMP2(full)/cc-pVDZ level and the total energies at the RMP2(full)/cc-pVDZ, RMP4-(SDTQ,full)/cc-pVTZ, and RQCISD(T,full)/cc-pVTZ levels for molecules in the $C_2H_5CHO \rightarrow C_2H_6 + CO$ reaction on the S_0 potential. In Table 3 are given the calculated and experimental values for the relative energies of this reaction. It is understood from this table that although the exothermicity predicted at the RMP2(full)/cc-pVDZ level is slightly larger than experiment, the barrier height calculated at this level is comparable with the barrier heights at the RMP4(SDTQ,full)/cc-pVTZ and RQCISD(T,full)/cc-pVTZ levels. Given the employed inexpensive theoretical method and basis set, the agreement with higher level theory might be still good and it should be reasonable to use the RMP2(full)/cc-pVDZ level for the current direct ab initio trajectory calculations.

Figure 1 displays the optimized geometries at the RMP2-(full)/cc-pVDZ level for propanal and the TS. Propanal has several conformers and the one in the figure is the cis conformer that lies in the lowest in energy according to the results of the previous ab initio MO calculations of other researchers.[35,44−47] It is noted that the current geometrical parameters of propanal

TABLE 3: Relative Energies Obtained by Theory and Experiment (kcal mol^{-1})

method	C_2H_5CHO	TS	$C_2H_6 + CO$	ref
RMP2(full)/cc-pVDZ//RMP2(full)/cc-pVDZ	0.0	86.1 (90.3)	−6.4 (−3.3)	present work
RMP4(SDTQ,full)/cc-pVTZ//RMP2(full)/cc-pVDZ	0.0	83.5 (87.7)	−3.5 (−0.5)	present work
RQCISD(T,full)/cc-pVTZ//RMP2(full)/cc-pVDZ	0.0	85.2 (89.4)	−2.6 (0.4)	present work
experiment	0.0		−1.3	43

[a] In parentheses are given the values without the ZPE correction.

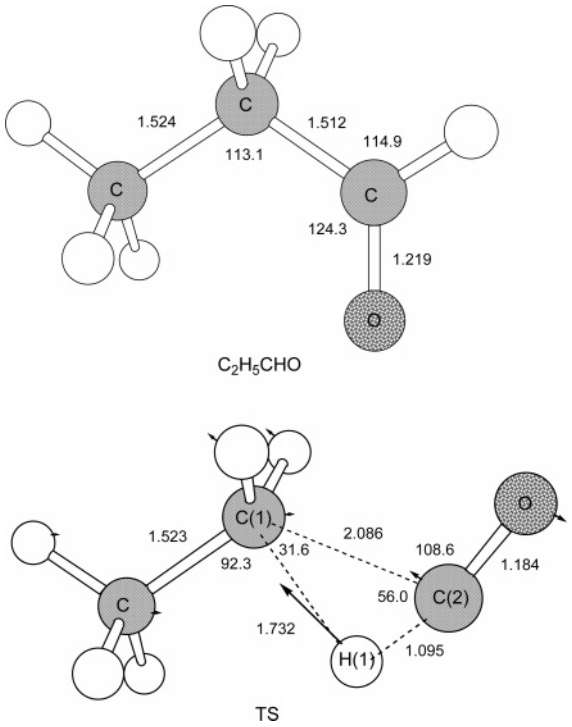

Figure 1. Optimized gepmetries obtained at the RMP2(full)/cc-pVDZ level for propanal (C_2H_5CHO) and the TS of the title reaction. The normal-mode vector of imaginary frequency for the TS is given in the figure. Bond lengths and angles are given in Å and degree.

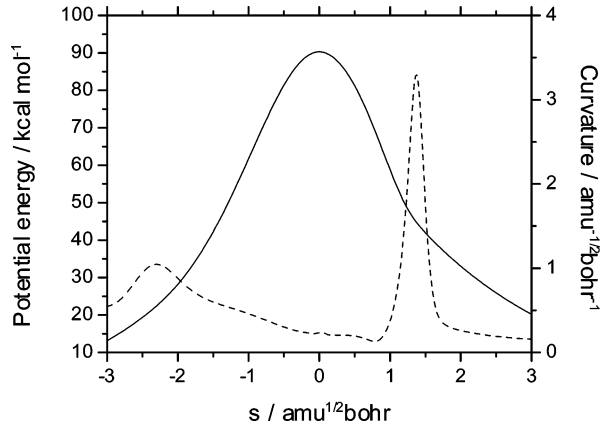

Figure 2. Potential energy profile (solid) and curvature (dashed) along the IRC: TS ($s = 0$); C_2H_5CHO ($s < 0$); $C_2H_6 + CO$ ($s > 0$).

are consistent with those of the previous calculations.[35,44−46] The vector of the TS imaginary vibrational mode is also given in the figure. Both the geometries have been predicted to have C_s symmetry and were confirmed to be at a minimum and saddle point on the potential surface, respectively, with the harmonic vibrational analyses presented in Table 1.

Figure 2 shows the potential energy profile along the IRC for the $C_2H_5CHO \rightarrow C_2H_6 + CO$ reaction; the TS is at $s = 0$ and the reactant C_2H_5CHO and products $C_2H_6 + CO$ are in the $s < 0$ and $s > 0$ regions, respectively, and the zero point of the potential energy is set to the total electronic energy of C_2H_5CHO. Also given in the figure is the curvature of the IRC. It is seen that the curvature takes its maximum of ~ 3.3 amu$^{-1/2}$ bohr^{-1} around $s = 1.4$ amu$^{1/2}$ bohr. It has been revealed that the curvature around this point is composed of one coupling constant between the IRC and a generalized normal mode that correlates with one of the vibrational modes of C_2H_6. It was also found that this generalized mode is contributed substantially by the H(1) motion. In our previous study,[19] we obtained the IRC curvature for the $CH_3CHO \rightarrow CH_4 + CO$ reaction that is almost the same as the current one, although the maximum of the curvature for this reaction is slightly smaller because of the difference in mass combination.

B. Product Energy Distribution. Final distributions of the product relative translational and internal energies for a total of ~700 trajectories are shown in Figure 3. Averaged energy values over the calculated trajectories are also given in the figure. The error-bar length Δp for event i of occurrence number n_i out of a sample of size n was approximately obtained by

$$\Delta p = \frac{2z}{n}\sqrt{n_i\left(1 - \frac{n_i}{n}\right)} \qquad (3)$$

where z (=1.96) is the 95% confidence value for the normal distribution.

Figure 3a shows the distribution of the relative translational energy and the averaged value is 36.3 kcal mol^{-1}. Parts b and c of Figure 3 give the distributions of the C_2H_6 and CO internal energies. The averaged C_2H_6 and CO internal energies are 112.8 kcal mol^{-1}, including the ZPE of 47.6 kcal mol^{-1}, and 23.2 kcal mol^{-1}, including that of 3.0 kcal mol^{-1}. Table 4 summarizes the available energies and averaged distributed energies obtained for the title reaction in this work. Also given in the table are the results for the $CH_3CHO \rightarrow CH_4 + CO$ reaction in our previous work.[19] Both the ZPE corrected and uncorrected values are given in the table. The averaged ZPE corrected distributed energies predicted for the relative translational motion, the C_2H_6 internal motion, and the CO internal motion in the propanal reaction are 36.3, 65.2, and 20.2 kcal mol^{-1}, respectively. It is of great interest to notice that the percentages of these distributed energies are very close to those for the relative translational motion, the CH_4 internal motion, and the CO internal motion in the acetaldehyde reaction. This seems surprising because the number of degree of freedom for C_2H_6 is larger than that for CH_4 and the percentage of the distributed energy for C_2H_6 should be expected larger than that for CH_4. Besides, the initial condition was generated microcanonically and the excess energy was equally distributed to all degrees of freedom when the trajectories started to move. The discussion on the energy-flow dynamics will be given in section 3D.

C. Product State Distribution. In this subsection, vibrational and rotational quantum states for the diatomic molecular product CO are discussed. The vibrational energy E_{vib} of CO was obtained from the summation of the kinetic energy for radial motion and the potential energy relative to the equilibrium position, both of which were calculated instantaneously from

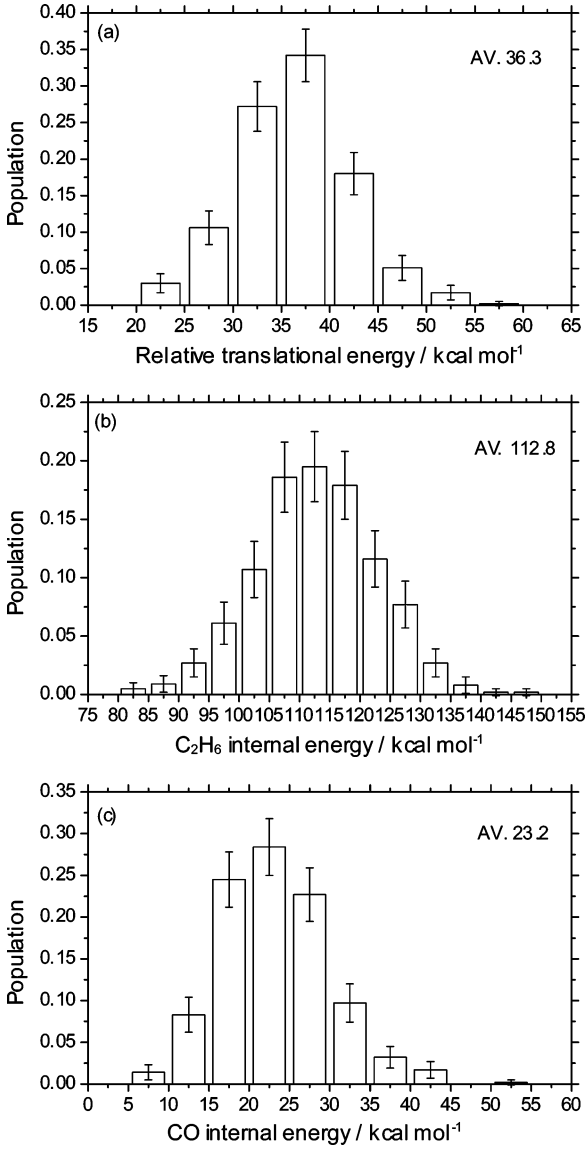

Figure 3. Product energy distributions: (a) relative translational energy; (b) C_2H_6 internal energy; (c) CO internal energy.

TABLE 4: Available and Averaged Final Distributed Energies (kcal mol^{-1})

this work	avail.	trans.	C_2H_6	CO
ZPE corrected	121.7	36.3 (29.8)[a]	65.2 (53.6)	20.2 (16.6)
per mode		12.1 (9.9)	3.1 (2.5)	6.7 (5.5)
ZPE uncorrected	172.3	36.3 (21.1)	112.8 (65.5)	23.2 (13.5)
per mode		12.1 (7.0)	5.4 (3.1)	7.7 (4.5)
previous work[19]	avail.	trans.	CH_4	CO
ZPE corrected	125.4	39.5 (31.5)	65.3 (52.1)	20.6 (16.4)
per mode		13.2 (10.5)	5.4 (4.3)	6.1 (4.9)
ZPE uncorrected	157.0	39.5 (25.2)	93.9 (59.8)	23.6 (15.0)
per mode		13.2 (8.4)	7.8 (5.0)	7.9 (5.0)

[a] In parentheses are given the percentages.

the data at the end of each trajectory. The rotational energy E_{rot} of CO was then determined as the difference between the total kinetic energy and the kinetic energy for radial motion. The vibrational quantum number n was obtained harmonically from

$$h\nu\left(n+\frac{1}{2}\right)=E_{vib} \tag{4}$$

and the rotational quantum number J from

$$\hbar^2 J(J+1)/2\mu r^2 = E_{rot} \tag{5}$$

where μ is the reduced mass and r the internuclear distance. Since the vibrational and rotational energies (and their quantum numbers) oscillate as a function of time because of the vibration−rotation coupling, it would be desirable to employ the time-averaged energies for obtaining these quantum numbers; this does not matter, however, when their distribution and average over many trajectories are discussed. Figure 4 shows the CO state distributions: (a) vibrational quantum number; (b) rotational quantum number. The CO vibrational quantum number is seen to range from 0 to 3, as shown in Figure 4a, and the averaged quantum number and vibrational energy are 0.36 and 5.2 kcal mol^{-1}, suggesting that the product CO is vibrationally cold. Figure 4b shows the distribution of the CO rotational quantum number. It is seen to range from 25 to 90 and the averaged quantum number and rotational energy are 57.6 and 18.0 kcal mol^{-1}, which indicates that the product CO is rotationally hot. The vibrationally cold and rotationally hot CO is generated because of the TS geometry and the normal-mode vector of the imaginary frequency at the TS; the vector can add some torque to CO but the CO bond in the TS is not so stretched. Although this explanation is based only on the property of the TS and not on the properties of other regions of potential surface, it seems reasonable because the coupling between the IRC and the degrees of freedom for CO was predicted to be small in the product region. The current result for the CO state distribution is quite similar to that obtained in our previous calculation.[19] This similarity arises form the similarity in the TS geometry and the vector of the imaginary frequency and from the very small coupling between the IRC and the degrees of freedom for CO.

D. Energy-Flow Dynamics. Figure 5a shows changes in averaged energy components as a function of time for the C_2H_5-CHO → C_2H_6 + CO reaction. $E_{C_2H_6}$, $E_{C_2H_6,vib}$, and $E_{C_2H_6,rot}$ are the total internal, vibrational, and rotational energies for the C_2H_6 fragment, respectively, and E_{CO}, $E_{CO,vib}$, and $E_{CO,rot}$ are those for the CO fragment. Note that these values were obtained by averaging instantaneous energies over all trajectories at each time step and that the internal energies $E_{C_2H_6}$ and E_{CO} include ZPE. Instantaneous rotational energy was obtained from

$$E_{rot}=\frac{1}{2}\mathbf{j}\mathbf{I}^{-1}\mathbf{j} \tag{6}$$

Here rotational angular momentum **j** and moment of inertia tensor **I** are given by

$$\mathbf{j}=\sum_i \mathbf{j}_i, \quad \mathbf{j}_i = m_i \mathbf{r}_i \times \dot{\mathbf{r}}_i \tag{7}$$

where m_i and $\mathbf{r}_i$ are the mass and position of atom i in a relevant molecule, and

$$\mathbf{I}=\begin{pmatrix} \sum_i m_i(y_i^2+z_i^2) & \sum_i m_i x_i y_i & \sum_i m_i x_i z_i \\ \sum_i m_i y_i x_i & \sum_i m_i(z_i^2+x_i^2) & \sum_i m_i y_i z_i \\ \sum_i m_i z_i x_i & \sum_i m_i z_i y_i & \sum_i m_i(x_i^2+y_i^2) \end{pmatrix} \tag{8}$$

Then the vibrational energy is given by the difference between the total internal energy and the rotational energy. E_{tra} is the relative translational energy for the two fragments. V_{int} is the

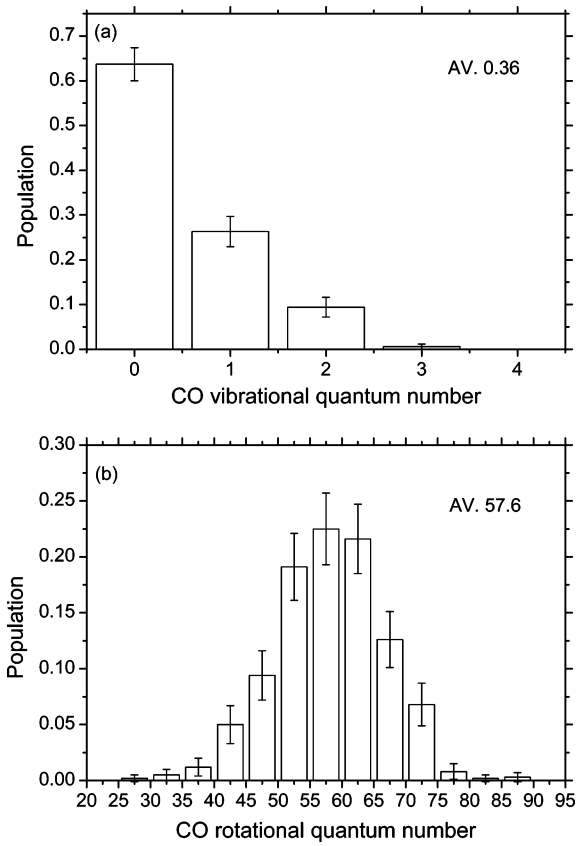

Figure 4. Product state distributions of CO: (a) vibrational quantum number; (b) rotational quantum number.

interaction energy between the two, obtained from $V_{int} = V_{total} - (V_{C_2H_6} + V_{CO})$, where V_{total} is the electronic energy of the total system, $V_{C_2H_6}$ is that of C_2H_6 at the same geometry as C_2H_6 in the total system, and V_{CO} is that of CO. For comparison, the same analysis was done for the acetaldehyde $CH_3CHO \rightarrow CH_4 + CO$ reaction using the data obtained in our previous study,[19] and the result is given in Figure 5b.

As shown in Figure 5a, V_{int} for the propanal reaction is positive when $t < \sim 40$ fs but is almost zero when $t > \sim 40$ fs. This means that the energy exchange among C_2H_6, CO, and their relative translational motion almost completes in the first 40 fs. It is seen that V_{int} has the maximum around $t = 5$ fs and this occurs because when t $< \sim$5 fs, V_{total} and V_{CO} do not change so much, while $V_{C_2H_6}$ decreases due to a rapid decrease in the internuclear distance C(1)−H(1), as shown in Figure 6a, and when $t > \sim$5 fs, $V_{C_2H_6}$ and V_{CO} oscillate, while V_{total} decreases due to a monotonic increase in the internuclear distance C(1)−C(2). As shown in Figure 6b, the internuclear distance C(1)−C(2) begins to increase around $t = 5$ fs, suggesting that V_{total} begins to decrease around this time. $E_{C_2H_6}$ is seen to oscillate when $t < \sim$40 fs; this is because in this time region the vibrating H(1) atom still interacts with the CO fragment and $E_{C_2H_6}$ is not conserved.

It is of interest to compare the changes in the energy components for the propanal reaction with those for the acetaldehyde reaction given in Figure 5b. It is seen that in this reaction V_{int} goes down to zero and E_{tra} reaches a plateau in the first 30 fs, while in the propanal reaction they do in the first 40 fs. This is because C_2H_6 is significantly heavier than CH_4 and it takes a longer time for the two fragments to get away from each other. Figure 6b demonstrates a difference between the propanal and acetaldehyde reactions in the increasing rate of the internuclear distance C(1)−C(2). It is also worth noting that

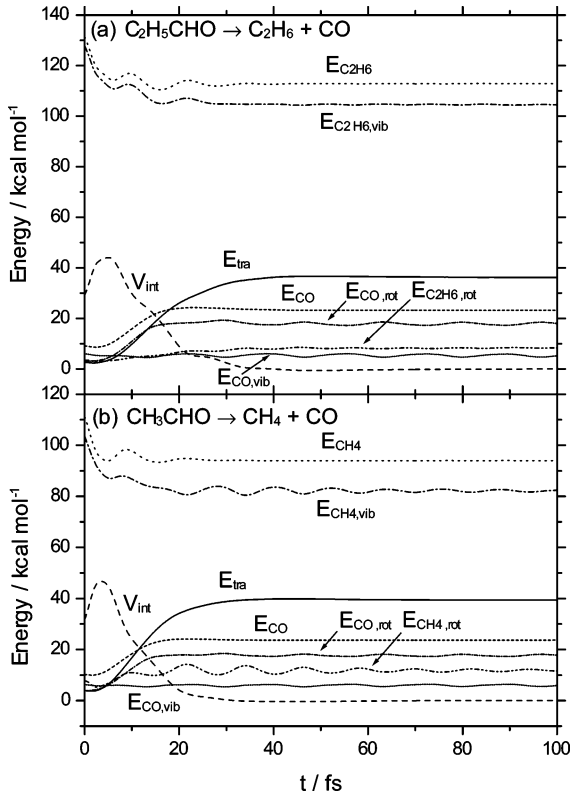

Figure 5. Changes in averaged energy elements as a function of time: (a) $C_2H_5CHO \rightarrow C_2H_6 + CO$; (b) $CH_3CHO \rightarrow CH_4 + CO$. E_A, $E_{A,vib}$, and $E_{A,rot}$ are the total internal, vibrational, and rotational energies, respectively, for fragment A. E_{tra} is relative translational energy for two fragments. V_{int} is interaction energy between two fragments. These values were obtained by averaging instantaneous ones over all trajectories at each time step.

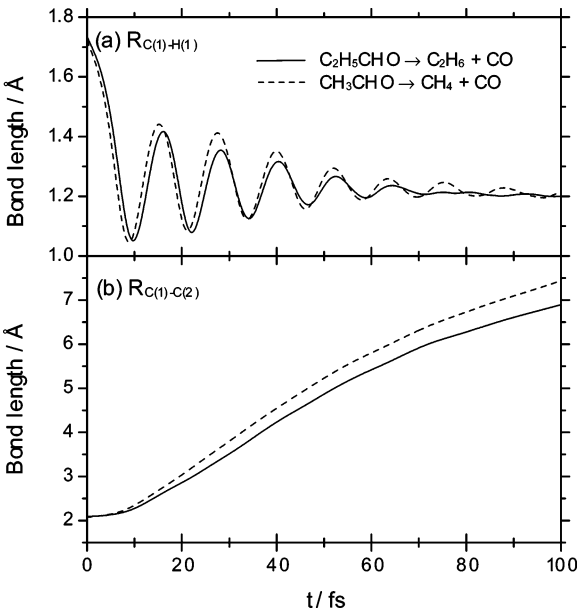

Figure 6. Changes in internuclear distances as a function of time for the propanal reaction: (a) C(1)−C(1); (b) C(1)−H(1). These values were obtained by averaging instantaneous ones over all trajectories at each time step.

$E_{CH_4,vib}$ and $E_{CH_4,rot}$ oscillate for a much longer time than $E_{C_2H_6,vib}$ and $E_{C_2H_6,rot}$; in general this oscillation is due to the rotation−vibration coupling. Since these values are averaged ones over all trajectories, disappearance of their oscillation means that the phase of vibration in each trajectory does not accord with one

another. Obviously, $E_{C_2H_6,vib}$ and $E_{CH_4,vib}$ mostly come from the H(1) motion; as displayed in Figure 6a, the oscillation of the averaged internuclear distance C(1)−H(1) for the propanal reaction disappears earlier than that for the acetaldehyde reaction, which accords well with the changes in $E_{C_2H_6,vib}$ and $E_{CH_4,vib}$. As pointed out above, the H(1) atom interacts with the CO fragment in the early stage of the reaction and the interaction time is substantially longer in the propanal reaction than in the acetaldehyde one. It is thought that the chances of the H(1) vibration being disturbed are higher in the propanal reaction because of its longer time interaction, which might lead to the difference in behaviors of E_{vib} and internuclear distance C(1)−H(1) between the two reactions.

In the current and previous[19] simulations, the propanal and acetaldehyde reactions were set to have about the same amount of available energy (see Table 4) and the excess energies were distributed microcanonically to all degrees of freedom at the initial condition. Of note is that the final energy distributions for the two fragments and their relative translational motion were found to be quite similar in these reactions despite the fact that the number of degree of freedom for C_2H_6 is larger than that for CH_4. At the initial condition the C_2H_6 fragment has the total internal energy of 84.1 kcal mol^{-1} and the CH_4 fragment has that of 82.6 kcal mol^{-1}, both of which exclude the ZPEs, and they are 69.1 and 65.9% of the available energy. E_{tra} and E_{CO} are only a few kcal mol^{-1} at the initial condition in both the reactions. It follows that 15.5 and 13.8% of the available energy flow out of C_2H_6 and CH_4, respectively; i.e., the percentage of the available energy that flows from C_2H_6 to the relative translational motion and to the CO fragment is about the same as that from CH_4 in the acetaldehyde reaction. In both the reactions, the coupling between the IRC and one of the generalized normal modes orthogonal to the IRC has been predicted quite strong around $s = 1.4$ amu$^{1/2}$ bohr; this generalized normal mode was found to be mostly composed of the H(1) motion. The predicted energy distributions strongly suggest that the coupling between this generalized normal mode and other modes in C_2H_6 is quite small and the intramolecular energy redistribution does not occur efficiently in this fragment; if it does, the percentage of the distributed energy for C_2H_6 should be larger than that for CH_4 in the acetaldehyde reaction. Thus, one conclusively states that in both the reactions the C(1)−H(1) bond is high in potential energy and this energy is released into the relative translational motion and into the CO fragment, hardly going into other modes of C_2H_6 or CH_4 due to their small coupling. On the basis of the discussion here, the same simulation for the molecular-channel photodissociation of a larger aldehyde such as $C_3H_7CHO \rightarrow C_3H_8 + CO$ would yield a final energy distribution that is similar to the present and previous ones.

In our previous study[19] for the acetaldehyde reaction, it was found that the final energy distribution is not so sensitive to the initial condition; the initial condition set microcanonically yields the same final energy distribution as the one obtained when the excess energy is added only to the reaction coordinate.[18] According to the result obtained in the present study, it is strongly expected that the initial internal energies given to the CH_4 fragment do not differ so much in the two cases because both their major portions are from the potential energy in the stretched C(1)−H(1) bond. As already revealed, there is a strong coupling between the IRC and a generalized normal mode that is mostly composed of the H(1) motion. Therefore, it is likely that the initial internal energy of the CH_4 fragment flows into the relative translational motion and into the CO fragment only through this coupling. Since this mechanism is common in the two cases, similar results for the energy distributions were obtained. Note that the coupling between the generalized normal mode and other modes in the CH_4 fragment is not needed to explain the similar final energy distributions, which is consistent with the result in the present study.

4. Conclusion

In this study we have carried out direct ab initio MD calculations for the molecular channel of the photodissociation of propanal, $C_2H_5CHO \rightarrow C_2H_6 + CO$, at 248 nm using the RMP2(full)/cc-pVDZ level of ab initio MO theory. The trajectories were started from the TS and the initial conditions were generated using the microcanonical sampling to put the excess energy randomly into all vibrational modes of the TS. A total of ∼700 trajectories were numerically integrated for 100 fs. As a result, the final energy distributions for the C_2H_6 and CO fragments and their relative translational motion were revealed to be quite similar to those obtained for the acetaldehyde reaction in our previous study despite the fact that the number of degrees of freedom for C_2H_6 is larger than that for CH_4. Since the C_2H_6 and CH_4 fragments were found to have about the same percentage of the available energy without ZPE at the initial condition, the present result indicates that the percentage of the available energy that flows out of C_2H_6 is about the same as that out of CH_4. In both the reactions, the coupling between the IRC and one of the generalized normal modes orthogonal to the IRC was predicted considerably strong at some point on the IRC in the product side and a detailed inspection showed that this generalized normal mode is significantly contributed by the H(1) motion. The predicted energy distributions strongly suggest that the coupling between this generalized normal mode and other modes in C_2H_6 is quite small and the intramolecular energy redistribution does not occur efficiently in this fragment; if it does, the percentage of the distributed energy for C_2H_6 should be larger than the present result. It is thus concluded that in both the reactions the potential energy in the stretched C(1)−H(1) bond is released into the relative translational motion and into the CO fragment, hardly going into other modes of C_2H_6 or CH_4 due to their small coupling.

Acknowledgment. Numerical calculations were carried out at Center for Promotion of Computational Science and Engineering in Japan Atomic Energy Agency, and we are grateful for their generous permission to use the SSCMPP system.

References and Notes

(1) Calvert, J. G.; Pitts, J. N., Jr. *Photochemistry*; John Wiley: New York, 1966.

(2) Finlayson-Pitts, B. J.; Pitts, J. N., Jr. *Atmospheric Chemistry: Fundamentals and Experimental Techniques*; John Wiley: New York, 1986.

(3) Campbell, I. M. *Energy and the Atmosphere: A Physical and Chemical Approach*, 2nd ed.; John Wiley: New York, 1986.

(4) Horowitz, A.; Kershner, C. J.; Calvert, J. G. *J. Phys. Chem.* **1982**, *86*, 3094.

(5) Horowitz, A.; Calvert, J. G. *J. Phys. Chem.* **1982**, *86*, 3105.

(6) Ohta, N.; Baba, H. *J. Phys. Chem.* **1986**, *90*, 2654.

(7) Kono, T.; Takayanagi, M.; Nishiya, T.; Hanazaki, I. *Chem. Phys. Lett.* **1993**, *201*, 166.

(8) Kono, T.; Takayanagi, M.; Hanazaki, I. *J. Phys. Chem.* **1993**, *97*, 12793.

(9) Terentis, A. C.; Stone, M.; Kable, S. H. *J. Phys. Chem.* **1994**, *98*, 10802.

(10) Lee, S.-H.; Chen, I.-C. *J. Chem. Phys.* **1996**, *105*, 4597.

(11) Gejo, T.; Bitto, H.; Huber, J. R. *Chem. Phys. Lett.* **1996**, *261*, 443.

(12) Lee, S.-H.; Chen, I.-C. *Chem. Phys.* **1997**, *220*, 175.

(13) Leu, G.-H.; Huang, C.-L.; Lee, S.-H.; Lee, Y.-C.; Chen, I.-C. *J. Chem. Phys.* **1998**, *109*, 9340.
(14) Huang, C.-L.; Chien, V.; Chen, I.-C.; Ni, C.-K.; Kung, A. H. *J. Chem. Phys.* **2000**, *112*, 1797.
(15) Gherman, B. F.; Friesner, R. A.; Wong, T.-H.; Min, Z.; Bersohn, R. *J. Chem. Phys.* **2001**, *114*, 6128.
(16) Huber, J. R. *Chem. Phys. Lett.* **2003**, *377*, 481.
(17) Cruse, H. A.; Softley, T. P. *J. Chem. Phys.* **2005**, *122*, 124303.
(18) Kurosaki, Y.; Yokoyama, K. *J. Phys. Chem. A* **2002**, *106*, 11415.
(19) Kurosaki, Y. *Chem. Phys. Lett.* **2006**, *421*, 549.
(20) Kurosaki, Y.; Yokoyama, K. *Chem. Phys. Lett.* **2003**, *371*, 568.
(21) Yadav, J. S.; Goddard, J. D. *J. Chem. Phys.* **1986**, *84*, 2682.
(22) King, R. A.; Allen, W. D.; Schaefer, H. F., III. *J. Chem. Phys.* **2000**, *112*, 5585.
(23) Cordeiro, M. N. D. S.; Martínez-Núñez, E.; Fernández-Ramos, A.; Vázquez, S. A. *Chem. Phys. Lett.* **2003**, *375*, 591.
(24) Thompson, K. C.; Crittenden, D. L.; Kable, S. H.; Jordan, M. J. T. *J. Chem. Phys.* **2006**, *124*, 044302.
(25) Garrison, W. M.; Burton, M. *J. Chem. Phys.* **1942**, *10*, 730.
(26) Blacet, F. E.; Pitts, J. N., Jr. *J. Am. Chem. Soc.* **1952**, *74*, 3382.
(27) Solomon, J.; Jonah, C.; Chandra, P.; Bersohn, R. *J. Chem. Phys.* **1970**, *55*, 1908.
(28) Shepson, P. B.; Heicklen, J. *J. Photochem.* **1982**, *19*, 215.
(29) Sodeau, J. R.; Beeby, A.; Whyte, L. J. *Spectrochim. Acta* **1990**, *46A*, 887.
(30) Martinez, J. R. D.; Buitrago, A. A.; Howell, N. W.; Hearn, C. H.; Joens, J. A. *Atmos. Environ.* **1992**, *26A*, 785.
(31) Terentis, A. C.; Knepp, P. T.; Kable, S. H. *J. Phys. Chem.* **1995**, *99*, 12704.
(32) Chen, Y.; Zhu, L. *J. Phys. Chem. A* **2001**, *105*, 9689.
(33) Metha, G. F.; Terentis, A. C.; Kable, S. H. *J. Phys. Chem. A* **2002**, *106*, 5817.
(34) Cordeiro, M. N. D. S.; Martínez-Núñez, E.; Fernández-Ramos, A.; Vázquez, S. A. *Chem. Phys. Lett.* **2003**, *381*, 37.
(35) Buntine, M. A.; Lee, C.; Metha, G. F. *Phys. Chem. Chem. Phys.* **2004**, *6*, 688.
(36) Frisch, M. J.; et al. *Gaussian 98*, Revision A.7; Gaussian, Inc.: Pittsburgh, PA, 1998.
(37) Peslherbe, G. H.; Wang, H.; Hase, W. L. *Adv. Chem. Phys.* **1999**, *105*, 171.
(38) Sun, L.; Hase, W. L. *J. Chem. Phys.* **2004**, *121*, 8831.
(39) Lindh, R. *Theor. Chim. Acta* **1993**, *85*, 423.
(40) El Azhary, A.; Rauhut, G.; Pulay, P.; Werner, H.-J. *J. Chem. Phys.* **1998**, *108*, 5185.
(41) Hampel, C.; Peterson, K.; Werner, H.-J. *Chem. Phys. Lett.* **1992**, *190*, 1 and references therein.
(42) Werner, H.-J.; Knowles, P. J.; Amos, R. D.; Bernhardsson, A.; Berning, Celani, P.; A.; Cooper, D. L.; Deegan, M. J. O.; Dobbyn, A. J.; Eckert, F.; Hampel, C.; Hetzer, G.; Korona, T.; Lindh, R.; Lloyd, A. W.; McNicholas, S. J.; Manby, F. R.; Meyer, W.; Mura, M. E.; Nicklass, A.; Palmieri, P.; Pitzer, R.; Rauhut, G.; Schütz, M.; Schumann, U.; Stoll, H.; Stone, A. J.; Tarroni, R.; Thorsteinsson, T. *MOLPRO, a package of ab initio programs*, version 2002.1.
(43) Afeefy, H. Y.; Liebman, J. F.; Stein, S. E. Neutral Thermochemical Data. In *NIST Chemistry WebBook, NIST Standard Reference Database Number 69*; Linstrom, P. J., Mallard, W. G., Eds.; June 2005, National Institute of Standards and Technology: Gaithersburg, MD (http://webbook.nist.gov).
(44) Klimkowski, V. J.; Van Nuffel, P.; Van Den Enden, L.; Van Alsenoy, C.; Geise, H. J.; Scarsdale, J. N.; Schafer, L. *J. Comput. Chem.* **1984**, *5*, 122.
(45) Metha, G. F.; Buntine, M. A.; McGilvery, D. C.; Morrison, R. J. S. *J. Mol. Spectrosc.* **1994**, *165*, 32.
(46) Durig, J. R.; Guirgis, G. A.; Bell, S.; Brewer, W. E. *J. Phys. Chem. A* **1997**, *101*, 9240.
(47) Vivier-Bunge, A.; Uc, V. H.; Smeyers, Y. G. *J. Chem. Phys.* **1998**, *109*, 2279.